Journal of Power Sources 194 (2009) 1164–1170

Contents lists available at ScienceDirect

Journal of Power Sources

journal homepage: www.elsevier.com/locate/jpowsour

Air electrode design for sustained high power operation of Li/air batteries

R.E. Williford*, Ji-Guang Zhang

Pacific Northwest National Laboratory, Richland, WA 99358, USA

ARTICLE INFO

Article history:
Received 27 April 2009
Received in revised form 28 May 2009
Accepted 3 June 2009
Available online 11 June 2009

Keywords:
Li/air battery
Carbon electrode
Porosity
Reaction precipitates
Catalyst distributions

ABSTRACT

The rapid development of portable electronic devices increasingly requires much more energy to support advanced functions. However, currently available batteries do not meet the high energy requirement of these devices. Metal/air batteries, especially Li/air batteries, have a much higher specific energy than most other available batteries, but their power rate is limited by the accumulation of reaction products in the air electrode. Several approaches to improve the power rate of Li/air batteries have been analyzed in this work, including adjustment of air electrode porosity and catalyst reactivity distributions to minimize diffusion limitations and maximize air electrode material utilization. An interconnected dual pore system (one catalyzed and one non-catalyzed) is proposed to improve oxygen transport into the inner regions of the air electrode, but this approach alone cannot supply high power for long term applications. A time-release multiple catalyst approach is analyzed to provide temporal release of reactivity in the air electrode. When coupled with the dual pore configuration and catalysts with high reactivities, the time-release catalyst concept can extend the duration of higher powers to longer times, and result in maximum utilization of air electrode materials.

1. Introduction

The most important advantage of metal–air batteries is that the active cathode material (oxygen) is not stored in the battery itself, but is absorbed from the surrounding environment during the discharge process. This unique property leads to a lighter and more compact battery. Of all the metal–air battery concepts (Fe, Zn, Al, Mg, Ca, and Li), the Li/air battery exhibits the highest theoretical capacity and specific energy 11,972 Wh kg^{-1} Li). Although the practical specific energy will be largely reduced after considering the weight of other components, it is still much larger than any other battery chemistry. Zheng et al. [1] calculated the theoretical capacities and energy densities per weight of air electrode for various aqueous (378–435 mAh g^{-1}, 1300–1400 Wh kg^{-1}) and non-aqueous electrolytes (940 mAh g^{-1}, 2790 Wh kg^{-1}) where the Li electrode, the air electrode (carbon), and the electrolyte are included in the weight. Other materials, such as membranes, the current collector, and package materials are not included in the calculation. The capacity reduction for aqueous electrolytes is due to the additional electrolyte inventory required to compensate for electrolyte consumption during discharge.

In a Li/air battery with a non-aqueous electrolyte [2], the cathodic reaction products (lithium oxide or peroxide) are not soluble in the electrolyte. The precipitation of these products in the pores of the air electrode (usually carbon based) reduces the available diffusion paths for oxygen, and the air electrode becomes oxygen starved as discharge progresses. Precipitation of reaction products (Li_2O or Li_2O_2) on the carbon pore surfaces (usually partially covered by catalyst particles) will reduce the activity of catalyst. Furthermore, these products often accumulate at or near the air-exposed surface of the air electrode, especially at high power conditions. Blocking of the air electrode surface prevents oxygen from reaching the interior regions of the air electrode, and air electrode material utilization is dramatically reduced [3–5].

The internal surface area and porosity of the air electrode [3,4] play important roles in the performance of Li/air batteries. Therefore, an optimized air electrode structure (e.g., with oxygen micro-channels and engineered porosity distribution) can significantly reduce oxygen starvation and improve air electrode utilization. The objective of the present paper is to explore several design alternatives for a porous air electrode to enable sustained higher power operation. Parameters available for exploration include the porosity distribution, pore connectivity, the tortuosity of the pore system, and the catalyst spatial distribution in the air electrode. The simulation model described below accounts for the effects of precipitate formation and the resulting pore blockage that causes oxygen starvation.

2. Model formulation

Fig. 1 shows a conceptual schematic of the Li/air battery discussed in this work. It shows a cross-section of a Li/air battery on

* Corresponding author. Tel.: +1 509 375 2956; fax: +1 509 375 2186.
E-mail address: Rick.Williford@pnl.gov (R.E. Williford).

0378-7753/$ – see front matter © 2009 Elsevier B.V. All rights reserved.
doi:10.1016/j.jpowsour.2009.06.005

Nomenclature

R	catalyst reactivity (reactions s^{-1})
D_0	diffusivity of oxygen in electrolyte ($m^2\ s^{-1}$)
D_i	diffusivity of oxygen in electrolyte in pore system i ($m^2\ s^{-1}$)
l_i	thickness of pore system i (m)
P_{O_2}	oxygen partial pressure (Pa)
ε	porosity
ε_0	initial porosity
C	oxygen concentration (mol m^{-3})
τ	tortuosity
τ_0	initial tortuosity
$\Delta\tau$	maximum change in tortuosity
f_ε	fraction of initial porosity that is catalyzed
f_i	volume fraction of catalyst in pore system i
t	time (s)
t_i	time delay for catalyst i (s)
F	oxygen fluence (mol m^{-3})
C_{sat}	oxygen saturation concentration (mol m^{-3})
ϕ	simulation factor for pore plugging

Subscripts

s	solid phase
g	gas phase
1	catalyzed pore subsystem
2	non-catalyzed pore subsystem
tot	total for both pore systems
0	initial value
i	catalyst type *i*

a plane normal to the Li foil anode. The battery is composed of a Li anode, a separator, a carbon-based air electrode, and a membrane to separate oxygen from atmospheric air. The oxygen 'micro-channels' that penetrate from the oxygen-exposed air electrode surface are intended to increase the air electrode surface area exposed to oxygen diffusion. A practical air electrode contains a mixture of micro- to nano-scale composite materials which allow oxygen to be transported to the interior of the electrode. A deliberate pattern of micro-channels can also be generated intentionally in an air electrode. In general, it is assumed that approximately two of the four sides of an arbitrary section of the air electrode will be exposed to oxygen, and this is approximated by the micro-channel geometry shown in Fig. 1. The cylindrical micro-channels are presumed to be placed in a square pattern with their long axes normal to the plane of the separator and the Li foil anode. The length:diameter aspect ratio of the micro-channels is about 20:1. The two-dimensional region of the air electrode to be addressed is shown as a textured rectangle in Fig. 1.

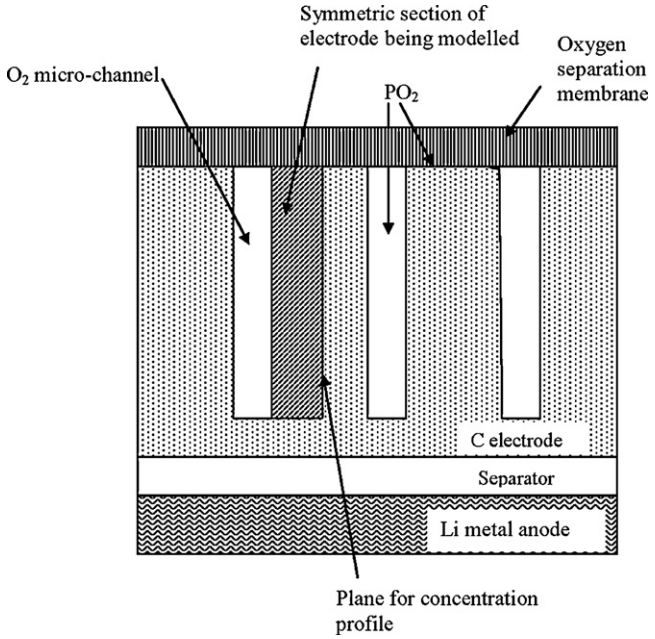

Fig. 1. Schematic cross-section of Li–air battery.

For clarity, the model is introduced in stages, from the simplest single pore system, to dual pore systems, to dual pore systems with multiple catalysts. The latter model is used for simulations. The primary phenomenon to be addressed is the diffusion limited behavior of the air electrode.

2.1. Single pore system

The assumptions for the model are common to those employed in previous publications [6], as follows. (a) Lithium ions are assumed to be present in the electrolyte, and to exhibit diffusivity through the electrolyte that is much larger than oxygen diffusivity. Thus, only the oxygen diffusion needs to be modeled. (b) The air electrode pores are assumed to contain metal oxide catalyst particles of unspecified species, with reactivity characterized by a constant R (reactions s^{-1}). R may be increased or decreased by either catalyst particle numbers or by using a different species of catalyst with different reactivity. (c) The primary chemical reaction is assumed to be first order with respect to dissolved oxygen concentration:

$$2Li_{(s)} + O_{2(g)} \Rightarrow Li_2O_{2(s)}. \quad (1)$$

The reaction product is assumed to be lithium peroxide. (d) The lithium peroxide reaction product is assumed to be insoluble in the organic electrolyte. The reaction product thus precipitates in the air electrode pores and reduces the porosity of the catalyzed air electrode, eventually stopping the transport of oxygen into and through the pores. (e) For a representative value, the diffusivity of oxygen in the electrolyte pore system is taken as $D_0 = 7 \times 10^{-10}\ m^2\ s^{-1}$ ($7 \times 10^{-6}\ cm^2\ s^{-1}$) [4] for 1 M $LiPF_6$ 1:1 PC:DME. D_0 is assumed to be constant. (f) The outer surface of the oxygen selective membrane is assumed to be exposed to room temperature air, with $P_{O_2} = 21,285$ Pa (0.21 atm). The air electrode surfaces defined by the micro-channel walls are assumed to be exposed to oxygen gas at the same partial pressure. (g) The oxygen selective membrane and the electrolyte are assumed to exclude water vapor from the air electrode pore system.

For simplicity, the reaction product was assumed to be lithium peroxide [6], although lithium oxide can occur depending on discharge rates and the electrolyte used [3]. The boundary and initial conditions are consistent with previous analyses [6]. The power was calculated from the flux of oxygen across the oxygen boundaries of the air electrode. This is the computational analogue of the experimental method used by Read [3]. The diffusivity of oxygen in the non-aqueous electrolyte was selected as a typical value from the literature [4], and the total porosity was constant at 70%, typical of a carbon air electrode.

A simple one-dimensional differential equation describing the diffusion of oxygen through the pore system, and its subsequent reaction in the pore system, is [7,8]

$$\frac{\partial(\varepsilon C)}{\partial t} = \frac{\partial}{\partial z}\left[D_O \frac{\varepsilon}{\tau}\frac{\partial C}{\partial z}\right] - RC \quad (2)$$

where C is the concentration (mol m^{-3}) of oxygen in the pore system, ε is the porosity and τ is the tortuosity of the pore system, and

t is time. The other variables have been described above. Although the time derivative on the left side of the equation, and the spatial derivative on the right side, account for changes in the porosity, the reaction rate R on the right side is a constant in Eq. (2). This implies that the reaction is unlimited, i.e., that the catalyst reactivity is not affected by the precipitation of the reaction products in the pores, even though the pores are eventually filled with reaction products. It is thus necessary to modify the differential equation to take this into account and to reflect a more realistic process in the air electrode. Because the diffusivity of oxygen through the precipitate is finite, and the thickness of the precipitate around a catalyst particle increases with time, the fluence (F, mol m^{-3}) of oxygen in the catalyzed pores is qualitatively expected to exhibit a damped exponential behavior as the pore fills with reaction product. An equation that describes this behavior is

$$F = C_{sat}(1 - e^{-(C/C_{sat})Rt}) \tag{3}$$

where C_{sat} is defined by the maximum oxygen concentration in the pore when this pore is blocked by lithium peroxide precipitate. C_{sat} is half the ratio of Li_2O_2 density per molecular weight. As time increases, the oxygen fluence (mol m^{-3}) in the pore increases towards the asymptotic value C_{sat}, at a rate defined by the reactivity R.

The process of pore filling by precipitates decreases the rate of oxygen diffusion into the pore as time progresses. Thus the unlimited reactivity defined by the term RC on the right side of Eq. (2) must be replaced by the rate at which oxygen is immobilized in the pore, or

$$\frac{dF}{dt} = C\ Re^{-CRt/C_{sat}} \tag{4}$$

The porosity correspondingly decreases according to the rate at which precipitates form in the pores:

$$\varepsilon = \varepsilon_0\ e^{-FRt/C_{sat}} \tag{5}$$

The pore becomes saturated when the fluence F of oxygen into the pore reaches the saturation value defined by the precipitate.

As the porosity decreases, the path oxygen must take to reach pores further into the interior becomes more circituous. The length of this path is generally described by the tortuosity [8]. The tortuosity of the pore system increases with fluence into the pores:

$$\tau = \tau_0 + \Delta\tau[1 - e^{-FRt/C_{sat}}] \tag{6}$$

where τ_0 and $\Delta\tau$ are the initial value and the maximum change in tortuosity, respectively.

These equations describe the behavior of a single pore system that contains a catalyst to promote the reaction between oxygen and lithium ions. The behavior of such a model is not surprising, and has been described by Sandhu et al. [6] for a single cylindrical pore. The inlet (mouth) of the pore becomes 'plugged' with reaction precipitate, severely restricting oxygen access to the interior region of the air electrode, and resulting in low utilization of the air electrode material along with reduced capacity for the battery. Power curves for this type of system are shown in a subsequent section of this paper.

2.2. Dual pore system in two dimensions

The air electrodes of Li/air batteries are manufactured from a variety of carbon sources, each exhibiting a network of pores that are interconnected to some degree. The air electrode can also be manufactured by mixing carbons from various sources, resulting in a dual set of pore systems that are presumably interconnected. If one pore system (carbon source) contains catalyst and the second pore system does not, only the catalyzed system will exhibit precipitation of reaction products. The second non-catalyzed pore system (presumably interconnected with the catalyzed pores) will remain open throughout the discharge process, so that oxygen can be delivered to the inner regions of the air electrode, thus improving material utilization and battery capacity. The equations given below describe such a dual pore system.

Diffusion through the two interconnected pore systems occurs in parallel (simultaneously), so the appropriate relationship for the overall diffusion coefficient is [7]:

$$l_1D_1 + l_2D_2 = l_{avg}D_{avg}. \tag{7}$$

Since the path lengths (l) are assumed approximately the same, the diffusivities simply add. Diffusivities must also be corrected for the porosity (ε) and tortuosity (τ) of each pore subsystem [8]:

$$D_i \rightarrow D_i\frac{\varepsilon_i}{\tau_i} \tag{8}$$

Assuming the catalyzed (non-catalyzed) pore system is denoted by the subscript 1 (2), the differential equation describing the transport of oxygen in a dual pore system for two spatial dimensions is thus:

$$\frac{\partial(\varepsilon_{tot}(t)C)}{\partial t} = -\nabla\cdot\left[-D_O\left(\frac{\varepsilon_1(t)}{\tau_1} + \frac{\varepsilon_2}{\tau_2(t)}\right)\nabla C\right] - \frac{dF}{dt} \tag{9}$$

where C is the concentration of oxygen in the total pore system, $\varepsilon_1(t)$ and ε_2 (τ_1 and $\tau_2(t)$) are the porosities (tortuosities) of the catalyzed and non-catalyzed pore systems, respectively, and $\varepsilon_{tot} = \varepsilon_1 + \varepsilon_2$ is the total porosity.

The fluence of oxygen into the catalyzed pore system is given by

$$F = f_\varepsilon CRe^{-CRt/f_\varepsilon C_{sat}} \tag{10}$$

where the factor

$$f_\varepsilon = \frac{\varepsilon_{10}}{\varepsilon_{10} + \varepsilon_{20}} \tag{11}$$

corrects the saturation concentration to that in the catalyzed pore system only, whereas the concentration C represents the entire pore system. This factor is approximated by the initial porosities (ε_{i0}) to prevent numerical singularities during the computer simulations described below. The equation for time-dependent changes in the porosity of the catalyzed system is

$$\varepsilon_1 = \varepsilon_{10}\ e^{-FRt/f_\varepsilon C_{sat}} \tag{12}$$

Precipitate blocking of the catalyzed pore system again requires the oxygen to take a more circituous path through the non-catalyzed pore system, because the two pore systems are presumed to be interconnected. The equation for the time-dependent changes in the tortuosity of the non-catalyzed pore system is thus

$$\tau_2 = \tau_{20} + \Delta\tau_2[1 - e^{-FRt/f_\varepsilon C_{sat}}] \tag{13}$$

Simulations for this type of pore system will be shown in a subsequent section.

2.3. Dual pore system with multiple time-release catalysts

It will be shown below that high battery power cannot be sustained for very long with the above microstructure. A third concept will thus be introduced, that of multiple time-release catalysts. These are envisioned as analogous to, e.g., time-release medications that contain coated particles. The time-release concept is also well known in the catalyst industry, e.g. [9–12], and has been called 'pastilef' in the literature on waxes. The coatings are dissolved (or in the present case, slowly penetrated by oxygen and subsequently cracked to expose the catalyst) at times proportional to the coating thicknesses. The intent is to control the power curve by delaying the rapid blocking of catalyzed pores at the beginning of battery discharge.

For the two-dimensional model given in Eq. (9), the fluence of oxygen in the catalyzed pores is given by

$$F = \sum F_i = f_\varepsilon C_{sat} \sum f_i [1 - e^{-R_i C(t-t_i)/f_\varepsilon C_{sat}}] \quad (14)$$

where f_i is the volume fraction of catalyst i in the catalyzed pore system with $\sum f_i = 1$, R_i is the reactivity of the given catalyst, and t_i is the time delay for catalyst i. Thus for multiple catalysts the oxygen depletion rate is given by

$$\frac{dF}{dt} = \sum \frac{dF_i}{dt} = C \sum f_i R_i \; e^{-\varphi R_i C(t-t_i)/f_\varepsilon C_{sat}} = f_i CR \quad \text{when} \quad \phi = 0. \quad (15)$$

The factor ϕ in the exponent has been added for convenience in simulating Case 1 below. $\phi = 0$ implies that the reaction precipitate does not plug the pore nor reduce the fluence into the pore with time, whereas $\phi = 1$ recovers the asymptotic effect of precipitates described above.

The differential equation for the changes in porosity of the catalyzed pore system is

$$\frac{d\varepsilon_1}{dt} = \sum f_i \frac{d\varepsilon_{1i}}{dt} = -\sum f_i R_i \varepsilon_{1i} \frac{F_i}{f_\varepsilon C_{sat}} \quad (16)$$

where

$$\varepsilon_{1i}(t=0) = f_i \varepsilon_{10}, \quad (17)$$

and the corresponding differential equation for changes in the tortuosity of the non-catalyzed pore system is

$$\frac{d\tau_2}{dt} = \sum \frac{d\tau_{2i}}{dt} = \Delta\tau_2 \sum \frac{f_i R_i F_i}{f_\varepsilon C_{sat}} e^{-F_i R_i (t-t_i)/f_\varepsilon C_{sat}} \quad (18)$$

where $\Delta\tau_2$ is the amount that τ_2 can increase due to plugging of the catalyzed pore system, with

$$\tau_{2i}(t=0) = f_i \tau_{20}. \quad (19)$$

Simulations for this type of pore/catalyst system are described below.

3. Results of simulations

Numerical simulations were performed using the finite difference method. A previously developed code [13,14] was available for this effort. Although written in FORTRAN 77, this code has the advantages of (a) a two-dimensional formulation, (b) treatment of the spatial variations in the effective diffusivities ($D_0\ \varepsilon/\tau$), so that both the time and spatial variations in porosity and tortuosity could be addressed, and (c) thorough testing and documentation. All calculations were performed with a relative error of 1×10^{-10}. The boundary conditions for Eq. (9) were Dirichlet type, i.e., $P_{O_2} = 21,285$ Pa for the oxygen-exposed surfaces at the top and left side of the textured model region shown in Fig. 1. All other boundary conditions were von Neumann type (zero gradient at the boundary) for all other variables (fluence F, porosity ε_1, and tortuosity τ_2 in Eqs. (15), (16), and (18)). The initial condition for Eq. (9) was $C(t=0) = 0$ over the entire region simulated. To simplify the discussion, $\Delta\tau_2 = 0.001$ was employed in Eq. (18), thus assuming good interconnection between the pore systems. Initial porosities and tortuosities are given below for each case. The diffusivity of oxygen in the electrolyte was $D_0 = 7 \times 10^{-10}$ m^2 s^{-1} as discussed above, and the voltage was assumed to be constant at 2.5 V (which is the average voltage in practical Li/air batteries). All calculations were performed for a 2-h potentiostatic discharge to simulate a field application that requires a constant voltage to operate equipment. The power was calculated from the flux of oxygen across the oxygen/air electrode boundaries at the interface between the oxygen selective membrane and the air electrode, and along the side of the oxygen micro-channel, as shown in Fig. 1. The dimensions of the section of air electrode being modeled in Fig. 1 were 5×10^{-4} m (500 μm) high by 4×10^{-5} m (40 μm) wide, divided into 11 and 4 nodes, respectively.

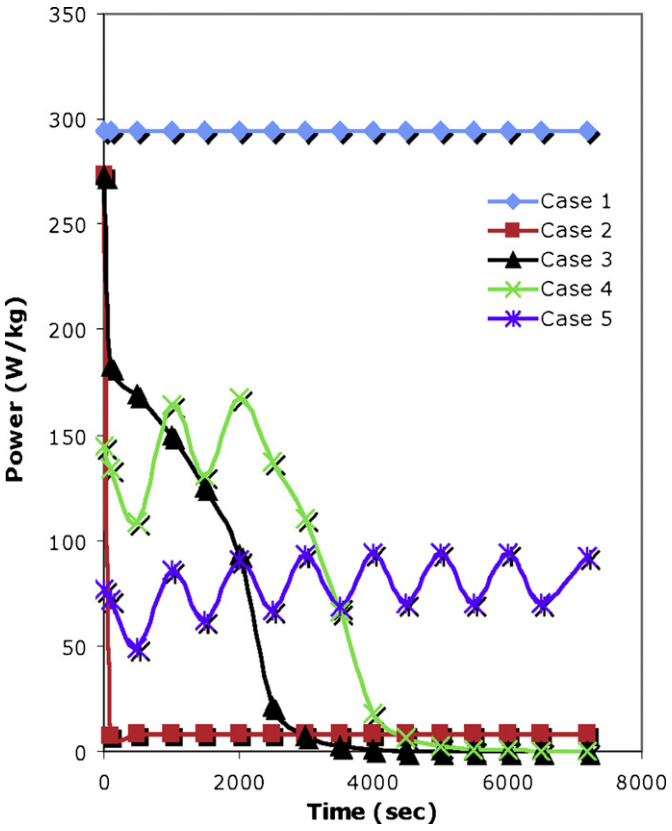

Fig. 2. Power curves versus time for the five cases described in the text.

The catalyst reactivity (R, reactions s^{-1}) was assumed to be 2.5. The battery powers shown below are only for *relative* comparisons between the results for the cases shown. This is sufficient for the present exploration of air electrode microstructural effects. The following series of cases were executed to allow comparisons between different microstructural designs for the air electrode.

Case 1: An approximate reference case with one catalyst ($N = 1$) for a 'nearly' single pore system with $\varepsilon_{10} = 0.69$, $\varepsilon_{20} = 0.01$ at $t = 0$. To eliminate the effect of pore blocking by formation of reaction precipitate, we set $\phi = 0.0$ and $d\varepsilon_1/dt = d\tau_2/dt = 0$. The selection of a finite (but small) porosity for the non-catalyzed pore system was necessary to prevent numerical singularities in Eq. (9) during the calculations. The (relative) power curve shown in Fig. 2 resembles the shape of classical voltage versus capacity curves under galvanostatic control, and is constant at 294 W kg^{-1} for 2 h because there is no pore blocking (only the weight of the carbon in the air electrode has been used in specific power and specific energy calculations in this work). For a 2 h discharge, the specific energy was 588 Wh kg^{-1} and the specific capacity was 235 Ah kg^{-1} (see Table 1). This case is actually not realistic because it does not consider pore blocking by precipitated reaction products. The case of a

Table 1
Energies and capacities after 2 h discharge for the cases simulated (weight refers to carbon used in the air electrode).

Case	Energy (Wh kg^{-1})	Capacity (Ah kg^{-1})
1	588	235
2	16.5	6.6
3	80	32
4	128	51
5	159	64

dual pore system ($\varepsilon_{10} = 0.35$, $\varepsilon_{20} = 0.35$) gave the same power curve, also because there was no pore blockage.

Case 2: A single pore system as in Case 1, but allowing for the formation of reaction precipitates ($\phi = 1.0$ and Eqs. (16) and (18) unchanged). The power falls rapidly to near zero (see Fig. 2) due to surface pore blockage by reaction precipitates, a result analogous to those reported by Sandhu et al. [6]. The specific energy and specific capacity were 16.5 Wh kg^{-1} and 6.6 Ah kg^{-1}, respectively (see Table 1).

Case 3: A dual pore system ($\varepsilon_{10} = 0.35$, $\varepsilon_{20} = 0.35$ with $\phi = 1.0$). The beneficial effect of the always-open non-catalyzed pore system is apparent. The specific energy and specific capacity of the battery for a 2-h discharge were 80 Wh kg^{-1} and 32 Ah kg^{-1}, respectively. The power is higher than in Case 2, but for a shorter duration than in the hypothetical Case 1.

In an attempt to extend the power curve to longer times, we explored a wide range of *spatial* distributions for the two porosities and for the catalyst, including layered systems of dual pore catalyzed and non-catalyzed carbons. However, the power curve could not be sustained at higher levels for more than about 1 h. The next alternative was to investigate the concept of time-release catalyst distributions, as follows.

Case 4: A dual pore system ($\varepsilon_{10} = 0.35$, $\varepsilon_{20} = 0.35$) with $\phi = 1.0$ and $N = 3$ time-release catalysts with $f_i = 1/3$ and release times of $t_i = 0$, 1000, and 2000 s. A higher power is maintained for about 3000 s, indicating that the concept could give favorable results. The specific energy and specific capacity were 128 Wh kg^{-1} and 51 Ah kg^{-1}, respectively for a 2-h discharge.

Case 5: This case is similar to Case 4 ($\varepsilon_{10} = 0.35$, $\varepsilon_{20} = 0.35$, $\phi = 1.0$), but with $N = 8$ time-release catalysts with $f_i = 1/8$ and $t_i = 0$, 1000, 2000, 3000, 4000, 5000, 6000, and 7000 s. The power is less than the three-catalyst simulation in Case 4 because the same total amount of catalyst has been partitioned between eight time-release catalysts, rather than three. Each time-release catalyst thus has a lower volume fraction. However, the power is indeed sustained for 2 h, indicating the potential value of the time-release catalyst concept for applications requiring sustained power at a constant potential to drive field devices. The specific energy and specific capacity were 159 Wh kg^{-1} and 64 Ah kg^{-1}, respectively.

Fig. 3 shows the oxygen concentration at 2 h of discharge as a function of distance along the center of the air electrode section (i.e., along the dashed vertical line at the right boundary of the textured model region in Fig. 1), normalized to the boundary concentration ($P_{O_2} = 21,285$ Pa or 0.21 atm). Depth/thickness = 0 corresponds to the oxygen selective membrane/air electrode interface at the top of the diagram, and depth/thickness = 1 corresponds to the carbon electrode at the bottom of the micro-channel Fig. 1. The hypothetical non-precipitating Case 1 with a single pore system and unlimited reaction capacity shows the concentration rapidly falling with distance into the air electrode, because the oxygen is consumed by reactions near the depth/thickness = 0 surface, in this case without penalty from precipitations.

The more realistic precipitating single pore system (Case 2) in Fig. 3 shows severe oxygen starvation in the interior regions of the air electrode due to precipitate formation at the surface (depth/thickness = 0), resulting in severe diffusion limitations for the bulk of the air electrode.

The realistic, precipitating dual pore system in Cases 3, 4, and 5 in Fig. 3 show that the always-open non-catalyzed pore system is efficient for transporting oxygen deeper into the air electrode. The oxygen concentration in Cases 3 and 4 is uniform across the electrode thickness because the non-catalyzed pore system is never blocked by precipitates. Case 5 shows lower concentration in the inner regions of the air electrode because the lower reactivity ($f_i R_i$) at a given time provides an oxygen 'sink' of lower intensity than in Cases 3 and 4, i.e., free oxygen is being continually removed from the pore system at a controlled rate in Case 5.

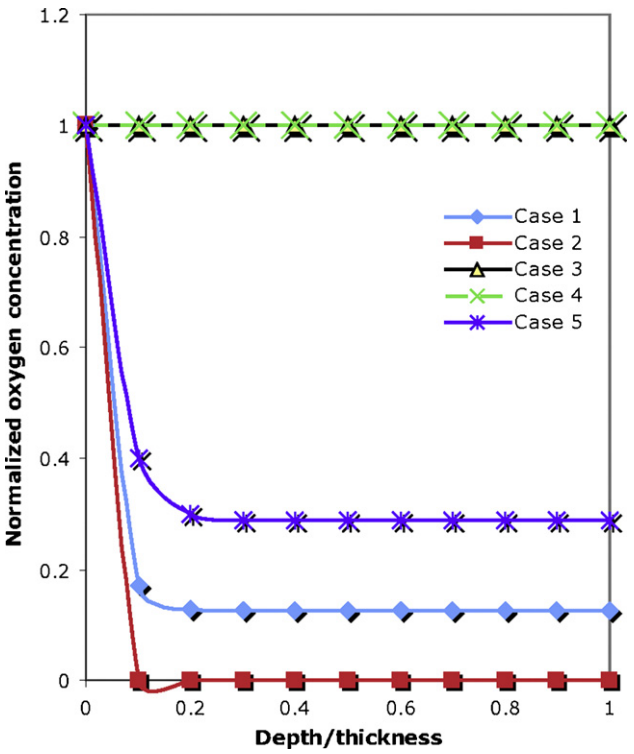

Fig. 3. Normalized concentration versus depth into the air electrode at 2 h of discharge. The curves are plotted at the position of the dashed vertical line in Fig. 1.

Fig. 4 is a plot of the normalized oxygen concentration at 2 h discharge versus the width and height (horizontal and vertical axes in Fig. 1) for Case 5. The oxygen-exposed boundaries are at the top (oxygen separator membrane) and left (microchannel surface) of Fig. 4. It can be seen that the oxygen gradient is approximately the same in both the vertical and horizontal directions, and the width of the modeled section is sufficient for decay of the oxygen concentration to low values at the position of the dashed vertical line in Fig. 1 (right side of Fig. 4). This is due primarily to the consumption

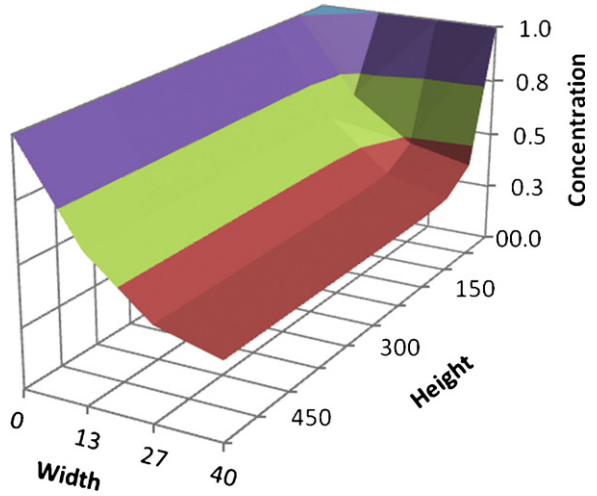

Fig. 4. Concentration profile for Case 5. The width axis is horizontal and the height axis is vertical in Fig. 1, and both are in units of microns to improve the readability of the plot. Concentrations are plotted vertically and are normalized to the boundary concentration. The highest concentrations (at the top of this figure) are defined by the boundary conditions.

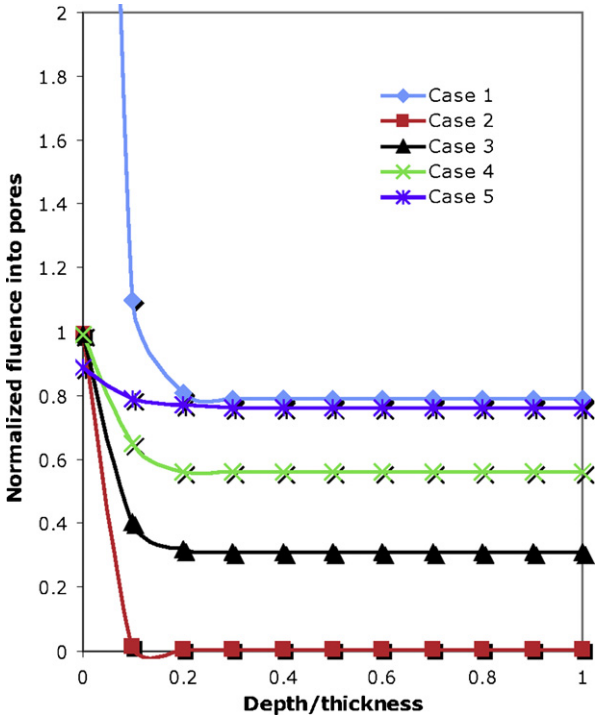

Fig. 5. Normalized filling of catalyzed pores versus depth into air electrode at 2 h of discharge.

of the oxygen by the reaction, which in turn reduces the effective diffusivity (Eq. (8)) by decreasing the porosity. The effect is severe even for temporally distributed catalysts, but less than for a single catalyst.

Fig. 5 shows the fluence F in the catalyzed pores (or the pore blocking) at 2 h discharge, normalized to the oxygen saturation concentration (C_{sat}) in the catalyzed pore system, again plotted versus the relative vertical depth into the air electrode. The hypothetical Case 1 exhibits surface pore oxygen fluence of over seven times C_{sat}, but because precipitation does not occur, more oxygen still reaches the inner regions of the air electrode to form reaction precipitates.

The realistic Case 2 with a single pore system shows that the blocking of surface pores causes oxygen starvation throughout most of the air electrode, resulting in poor material utilization.

The realistic dual pore systems in Cases 3–5 of Fig. 5 show increasing material utilization as the number of time-release catalysts is increased, thus distributing the reactivity and precipitates over space and time. In particular, the utilization of material in Case 5 approaches that in Case 1 in the interior regions of the air electrode. Increasing the number of time-release catalysts extends the power curve, but also reduces the power level because of conservation of catalyst mass ($\sum f_i = 1$). The power curve could be raised to a higher level by employing catalysts with higher reactivities R_i.

4. Discussion and conclusions

Despite the advantage of high specific energy, the performance of the Li/air battery is limited by the insolubility of the reaction products in non-aqueous electrolytes. This causes precipitation of the reaction products in the air electrode pores, which in turn blocks the passage of oxygen to the inner regions of the air electrode. The result is low material utilization in the air electrode, capacity less than theoretical, and severe restrictions on the duration of high power output.

The most desirable solution to this problem is the development of an electrolyte with high solubility for reaction products. An alternative solution, the subject of this paper, is to manipulate the porosity and catalyst distributions within the air electrode so that higher powers can be achieved for longer times. The model developed in this paper addresses this problem.

The basic reaction–diffusion differential equation is well founded in the technology of porous catalysts. Although presently limited to two-dimensional simulations, no important qualitative differences are expected for three-dimensional treatments. Differential equations for the evolution of precipitate accumulation in the pores, the decrease of porosity, and the increase of tortuosity as the diffusion–reaction process progresses during discharge, can be considered somewhat heuristic, due to the lack of reliable data for, e.g., the diffusivity of oxygen through the reaction products that precipitate in the pores. However, these equations capture the basic characteristics of these phenomena, and are thus considered useful for this initial investigation. Because the catalyst reactivity (R, reactions s^{-1}) is assumed but not calibrated due to lack of suitable experimental data, the model can *only* be used for *relative* comparisons of the effects of various microstructural configurations in the air electrode material. Data for reactivities will be needed to benchmark the model to specific air electrode/electrolyte/catalyst combinations.

The dual pore concept has been used in catalyst technology, and is composed of two interconnected porosity systems: one that is catalyzed and one that is not catalyzed. The non-catalyzed system ensures transport of oxygen into the air electrode even when the catalyzed system becomes blocked by reaction precipitates. Dual pore air electrodes could be manufactured by mixing or layering two batches of porous carbons: one catalyzed and the other non-catalyzed. The proposed time-release catalyst concept is familiar in the drug and catalyst industries, but is a new concept for battery technologies.

Conclusions that can be drawn from the results of simulations are as follows.

- The dual pore system offers advantages for improved oxygen transport into the inner regions of the air electrode. However, no spatial distributions of porosity or catalyst reactivity could be found that would provide high battery power for extended operation.
- The proposed multiple time-release catalyst scenario is a temporal distribution of reactivity in the air electrode. When coupled with the dual pore configuration, time-release catalysts can extend the duration of higher powers to longer times, and result in air electrode material utilization that is comparable to theoretical cases with no precipitation of reaction products and no pore blocking. Although the peak power was reduced because the catalyst mass (or total reactivity) was conserved in these simulations, catalysts with higher reactivities would allow higher peak powers to be sustained over longer times.

Acknowledgements

This work was approved for Public Release, Distribution Unlimited. Pacific Northwest National Laboratory is operated by Battelle Memorial Institute for the US Department of Energy.

References

[1] J.P. Zheng, R.Y. Liang, M. Hendrickson, E.J. Plichta, J. Electrochem. Soc. 155 (2008) A432–A437.
[2] K.M. Abraham, Z. Jiang, J. Electrochem. Soc. 143 (1996) 1–5.
[3] J. Read, J. Electrochem. Soc. 149 (2002) A1190–A1195.

[4] J. Read, K. Mutolo, M. Ervin, W. Behl, J. Wolfenstine, A. Driedger, D. Foster, J. Electrochem. Soc. 150 (2003) A1351–A1356.
[5] Kowaluk, J. Read, M. Saloman, Pure Appl. Chem. 79 (2007) 851–860.
[6] S.S. Sandhu, J.P. Fellner, G.W. Brutchen, J. Power Sources 164 (2007) 365–371.
[7] J. Crank, The Mathematics of Diffusion, Oxford University Press, 1975 (Chapter 14).
[8] R. Aris, The Mathematical Theory of Diffusion and Reaction in Permeable Catalysts, vol. 1, Clarendon Press, Oxford, UK, 1975, pp. 50–53.
[9] Z.H. Qin, M. Lewandowski, Y.N. Sun, et al., J. Phys. Chem. C 112 (2008) 10209–10213.
[10] N. Isiklan, M. Inal, Yigitoglu, J. Appl. Polym. Sci. (2008) 481–493.
[11] M. Inal, M. Yigitoglu, N. Isiklan, E-Polymers (2008), Article Number 017.
[12] M. Prokopowicz, J. Lukasiak, A. Przyjazny, J. Biomater. Sci.-Polym. Ed. 15 (2004) 343–356.
[13] D.K. Melgaard, R.F. Sincovec, ACM Trans. Math. Software 7 (1981) 106–125.
[14] R.F. Sincovec, N.K. Madsen, ACM Trans. Math. Software 1 (1975) 232–260.